
Article:
Linse, T., Hennig, P., Kaestner, M. et al. (1 more author) (2017) A convergence study of phase-field models for brittle fracture. Engineering Fracture Mechanics, 184. pp. 307-318. ISSN 0013-7944

https://doi.org/10.1016/j.engfracmech.2017.09.013

A convergence study of phase-field models for brittle fracture

Thomas Linse[a], Paul Hennig[a], Markus Kästner[a,b], René de Borst[c,*]

[a] *Technische Universität Dresden, Institute of Solid Mechanics, Chair of Computational and Experimental Solid Mechanics, 01062 Dresden, Germany*
[b] *Technische Universität Dresden, Dresden Center for Computational Materials Science (DCMS), 01062 Dresden, Germany*
[c] *University of Sheffield, Department of Civil and Structural Engineering, Mappin Street, Sir Frederick Mappin Building, Sheffield S1 3JD, UK*

Abstract

A crucial issue in phase-field models for brittle fracture is whether the functional that describes the distributed crack converges to the functional of the discrete crack when the internal length scale introduced in the distribution function goes to zero. Theoretical proofs exist for the original theory. However, for continuous media as well as for discretised media, significant errors have been reported in numerical solutions regarding the approximated crack surface, and hence for the dissipated energy. We show that for a practical setting, where the internal length scale and the spacing of the discretisation are small but finite, the observed discrepancy partially stems from the fact that numerical studies consider specimens of a finite length, and partially relates to the irreversibility introduced when casting the variational theory for brittle fracture in a damage-like format. While some form of irreversibility may be required in numerical implementations, the precise form significantly influences the accuracy and convergence towards the discrete crack.

Keywords: Phase-field model, Fracture, Damage, Gamma convergence

*Corresponding author: René de Borst
Email address: r.deborst@sheffield.ac.uk (René de Borst)

1. Introduction

Discrete models, in which the original geometry is modified during the computation to account for the propagation of a discontinuity are intuitive, and improvements such as remeshing (Wawrzynek and Ingraffea, 1987; Camacho and Ortiz, 1996; Secchi et al., 2007) and extended finite element methods (Belytschko and Black, 1999; Moës et al., 1999; Wells et al., 2002; de Borst et al., 2006) have provided ways to decouple the path of a propagating discontinuity from the original discretisation. Still, issues remain, such as the proper modelling of curved interfaces in three dimensions, and the robust implementation in three dimensions, which is a non-trivial task, neither when using remeshing, nor when exploiting the partition of unity concept as in extended finite elements. These drawbacks have promulgated the development and use of distributed, or smeared approaches, where the discontinuity is distributed over a finite width.

In this context, phase-field models have become increasingly popular for simulating a host of physical phenomena which exhibit sharp interfaces. Examples are the modelling of solidification processes, spinodal decomposition, coarsening of precipitate phases, shape memory effects, re-crystallisation, and dislocation dynamics, see e.g., Chen (2002); Emmerich (2008); Moelans et al. (2008); Steinbach (2009); Kästner et al. (2016) for overviews. The central idea behind phase-field models is that a discontinuous interface – where a Heaviside function placed at the interface models the jump in the primary variable – is replaced by a smooth function with a steep slope locally. This implies that in the gradients of the primary variable, the Dirac delta function is replaced by a regularised Dirac function, Figure 1.

The application of phase-field models to fracture is particularly interesting and challenging. Pioneering work has been done by Francfort and Marigo (1998); Bourdin et al. (2008), who proposed a phase-field approximation of the variational formulation for Griffith's theory of brittle fracture based on the Mumford-Shah potential (Mumford and Shah, 1989). A numerical implementation and examples were provided in Bourdin et al. (2000); Bourdin (2007). In this so-called variational approach to brittle fracture a sharp crack is distributed over a small, but finite width, that is proportional to an internal length scale ℓ, Figure 1. Accordingly, the fracture energy, i.e. the energy that is needed to create a unit area of fully developed crack, is distributed over a finite zone. In this variational approach to brittle fracture, gradients are included in the functional, similar to gradient-enhanced damage mod-

els (de Borst et al., 1996; Frémond and Nedjar, 1996; Peerlings et al., 1996). The point of departure of both models, however, is different. In gradient damage models a mechanical approach is followed, and the damage model is regularised by adding gradients to restore well-posedness of the boundary value problem in the post-peak regime. The basic idea of phase-field models, on the other hand, is to replace the zero-width discontinuity by a small, but finite zone with sharp spatial gradients in a mathematically consistent manner.

More recently, Miehe and co-workers (Miehe et al., 2010a,b) have exploited the similarities between phase-field theories for brittle fracture and gradient-enhanced damage models to cast phase-field models for brittle fracture in a damage format by explicitly utilising notions like a degradation function, and a damage loading function to set the irreversibility of damage. Indeed, the phase-field variable was interpreted in a manner that is synonymous to the damage variable in scalar-based damage models, starting at zero for a virgin material, and monotonically increasing to one when the material has lost all coherence. Recently, it has been shown that this formulation of the phase-field model for brittle fracture can be made identical to gradient-based damage models for a particular choice of the damage degradation function, the diffusion equation that governs the spread of the damage, and the material functions (de Borst and Verhoosel, 2016). Phase-field models have now been applied to a variety of fracture problems, including dynamic fracture (Borden et al., 2012; Hofacker and Miehe, 2013), cohesive fracture (Verhoosel and de Borst, 2013), and finite deformations (Hesch et al., 2017).

A crucial issue in the phase-field approach to brittle fracture is the requirement that the functional Π_ℓ, which describes the distributed crack surface, approaches the functional Π for the discrete crack for $\ell \to 0$. When $\Pi_\ell \to \Pi$ for $\ell \to 0$, the size Γ_ℓ of the smeared crack converges to the size Γ of the discrete crack. For a continuous medium such a proof exists (Chambolle, 2004), and in Bellettini and Coscia (1994) this proof has been given for a discrete medium, i.e. $\Pi_{\ell,h}$ converges to Π for $\ell \to 0$ under the condition that $h \ll \ell$, where h is the mesh spacing. Doubt has been cast on whether Γ-convergence can be achieved in actual computations, since, using the phase-field model for brittle fracture as developed by Miehe et al. (2010a,b), Vignollet et al. (2014) and May et al. (2015) have shown by numerical analyses of some simple boundary value problems that there exists a ratio ℓ/h for which the difference $|\Gamma_\ell - \Gamma|$ attains a minimum. Moreover, at this minimum the error

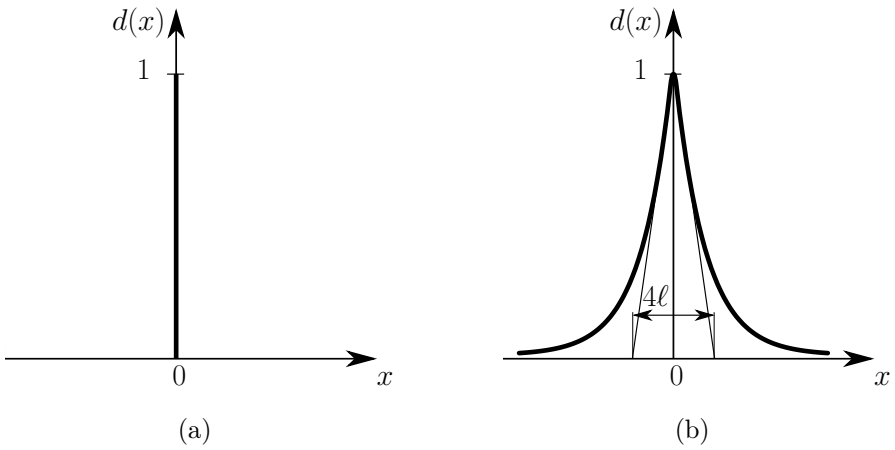

Figure 1: (a) A sharp discontinuity, and (b) distributed discontinuity, smeared using the length scale parameter ℓ.

can amount to values of $15-20\%$, suggesting a significant error even for the optimal discretisation.

Herein, we will show that this discrepancy is related to boundary effects, i.e. the effect of a specimen of a finite size, and to the introduction of a history variable that enforces irreversibility of the damage evolution. The convergence proofs (Chambolle, 2004; Bellettini and Coscia, 1994) are for the original variational formulation of Griffith's theory (Francfort and Marigo, 1998), including its regularised form (Bourdin et al., 2000), where the phase-field parameter merely serves as an order parameter, and is not given the role of a history variable as in Miehe et al. (2010a,b).

To provide a proper setting we start by giving a brief outline of the phase-field representation of a discontinuity, and the phase-field model for brittle fracture. This is followed by an in-depth numerical analysis of a simple, but illustrative one-dimensional problem, which provides detailed information and serves to fully explain the observed discrepancy. Concluding remarks complete the paper.

2. The phase-field approach to brittle fracture

2.1. Phase-field representation of a discontinuity

The basic idea of phase-field models is to approximate a discontinuity Γ by a smeared surface Γ_ℓ. In a one-dimensional setting the exponential

function

$$d(x) = \mathrm{e}^{-\frac{|x|}{2\ell}} \tag{1}$$

is used to approximate the discontinuous function of Figure 1(a), with ℓ being the internal length scale parameter. The phase-field variable $d \in [0, 1]$ describes the phase-field such that $d = 0$ characterises the intact state of the material, while $d = 1$ represents the fully broken material, similar to the definition commonly adopted in damage mechanics. In one dimension, Equation (1) is the solution to:

$$d - 4\ell^2 d_{,xx} = 0 \ , \tag{2}$$

where a comma denotes differentiation. Equation (2) is subject to the boundary conditions:

$$d(0) = 1 \text{ and } d(\pm\infty) = 0 \ . \tag{3}$$

Using Euqation (2), the discontinuity Γ can be approximated by the functional Γ_ℓ

$$\Gamma_\ell = \int_\Omega \underbrace{\frac{1}{4\ell}\left(d^2 + 4\ell^2 {d_{,x}}^2\right)}_{\gamma_\ell} \, \mathrm{dV} \ , \tag{4}$$

with γ_ℓ being the crack surface density function, see Miehe et al. (2010b) for details. In a one-dimensional setting the approximation is exact:

$$\Gamma_\ell = \int_{-\infty}^{+\infty} \frac{1}{4\ell}\left(d^2 + 4\ell^2 {d_{,x}}^2\right) A \mathrm{dx} = A = \Gamma \ , \tag{5}$$

where A is the cross section of the bar. In a multi-dimensional setting Γ_ℓ can be expanded as follows:

$$\Gamma_\ell = \int_\Omega \frac{1}{4\ell}\left(d^2 + 4\ell^2 \nabla d \cdot \nabla d\right) \, \mathrm{dV} \ . \tag{6}$$

2.2. Application to brittle fracture

We next consider a volume Ω with an internal discontinuity boundary Γ. As a starting point we consider the energy functional for brittle fracture in a Griffith sense (Francfort and Marigo, 1998):

$$\Pi = \int_\Omega \psi^e(\boldsymbol{\epsilon}) \, \mathrm{d}V + \int_\Gamma \mathcal{G}_c \, \mathrm{dA} \ , \tag{7}$$

where the elastic energy density ψ^e is a function of the infinitesimal strain tensor $\boldsymbol{\epsilon}$: $\psi^e = \psi^e(\boldsymbol{\epsilon})$. The elastic energy density is expressed by Hooke's law for an isotropic linear elastic material as $\psi^e(\boldsymbol{\epsilon}) = \frac{1}{2}\lambda\epsilon_{ii}\epsilon_{jj} + \mu\epsilon_{ij}\epsilon_{ij}$, with λ and μ being the Lamé constants, and the summation convention applies. In Equation (7) the fracture energy density is denoted by $\mathcal{G}_c$. In the spirit of a regularised crack topology, the work $\mathcal{W}_c$ required to create a cracked area Γ is expressed as a volume integral which depends on the phase-field variable d and the fracture energy density $\mathcal{G}_c$:

$$\mathcal{W}_c = \int_\Gamma \mathcal{G}_c \,\mathrm{dA} \approx \int_\Omega \mathcal{G}_c \gamma_\ell(d, \nabla d) \,\mathrm{dV} \ . \tag{8}$$

The next step is inspired by damage mechanics concepts and relies on the assumption that the evolution of the phase-field is directly related to crack growth. As such, it can be thought of as a way to model the loss of stiffness of the bulk of the solid. For this purpose a degradation function $g = g(d)$ is introduced, which must meet the following requirements:

$$\begin{cases} g : [0,1] \to [0,1] \\ g(0) = 1, \quad g(1) = 0 \\ g'(d) < 0, \quad d \in [0,1[\\ g'(1) = 0 \ . \end{cases} \tag{9}$$

These properties ensure damage propagation and provide an upper bound to the phase-field variable (Miehe et al., 2010a). A simple function that satisfies the above conditions is the quadratic polynomial:

$$g(d) = (1-d)^2 \ . \tag{10}$$

It is emphasised that, while the crack has been distributed in Equation (8) using mathematical arguments, the introduction of a degradation function $g(d)$ is heuristic, inspired by a phenomenological concept commonly used in damage mechanics.

Damage evolution can occur under different straining modes (Amor et al., 2009; Miehe et al., 2010b) and it is therefore assumed that the elastic energy of the undamaged state can be decomposed into a damaged and an intact part, such that the degradation function $g(d)$ only acts on the damaged part:

$$\psi^e(\boldsymbol{\epsilon}, d) = g(d)\psi^d(\boldsymbol{\epsilon}) + \psi^i(\boldsymbol{\epsilon}) \ . \tag{11}$$

Substitution of Equations (8) and (11) into Equation (7) yields the total potential energy for distributed brittle fracture:

$$\Pi_\ell = \int_\Omega \left(g(d)\psi^d(\boldsymbol{\epsilon}) + \psi^i(\boldsymbol{\epsilon}) + \mathcal{G}_c \gamma_\ell(d, \nabla d) \right) \, \mathrm{dV} \ . \tag{12}$$

At this point, again borrowing a concept from damage mechanics, a history field $\mathcal{H}$ (commonly denoted by κ in damage mechanics) is introduced to enforce irreversibility (Miehe et al., 2010a). Minimisation of Π_ℓ then leads to the equilibrium equation:

$$\operatorname{div} \boldsymbol{\sigma} = \mathbf{0} \tag{13}$$

and to

$$g'(d)\mathcal{H} + \frac{\mathcal{G}_c}{2\ell} \left(d - 4\ell^2 \nabla^2 d \right) = 0 \ , \tag{14}$$

subject to the boundary conditions

$$\mathbf{n} \cdot \boldsymbol{\sigma} = \bar{\mathbf{t}}, \ \mathbf{u} = \bar{\mathbf{u}} \tag{15}$$

and

$$\mathbf{n} \cdot \nabla d = 0, \tag{16}$$

where $\bar{\mathbf{t}}$ and $\bar{\mathbf{u}}$ are the prescribed boundary tractions and displacements, respectively. Alternatively, irreversibility can be enforced by setting $d = 1$ when d approaches one (Bourdin et al., 2000; Kuhn and Müller, 2010). The Cauchy stress $\boldsymbol{\sigma}$ and the driving force $\mathcal{F}$ are derived according to standard thermodynamic arguments:

$$\boldsymbol{\sigma} = \frac{\partial \psi^e}{\partial \boldsymbol{\epsilon}} = g(d) \frac{\partial \psi^d}{\partial \boldsymbol{\epsilon}} + \frac{\partial \psi^i}{\partial \boldsymbol{\epsilon}} \tag{17}$$

and

$$\mathcal{F} = -\frac{\partial \psi^e}{\partial d} = -g'(d)\mathcal{H} \ , \tag{18}$$

with ψ^e as defined in Equation (11). The history field is defined as the maximum damaged part of the energy density obtained in time history:

$$\mathcal{H} = \max_{s \in [0;t]} \psi^d(\boldsymbol{\epsilon}, s) \ . \tag{19}$$

For $\psi^d = \psi^e$ and $\psi^i = 0$, Γ-convergence can be shown when the functional Π_ℓ of the distributed crack converges to the discrete crack functional Π in

Equation (7) for $\ell \to 0$, i.e.

$$\Pi_\ell\big|_{\ell\to 0} = \left(\int_\Omega g(d)\psi^e \,\mathrm{dV} + \int_\Omega \mathcal{G}_c \gamma_\ell \,\mathrm{dV} \right) \Big|_{\ell\to 0} = \int_\Omega \psi^e \,\mathrm{dV} + \int_\Gamma \mathcal{G}_c \,\mathrm{dA} = \Pi \ . \tag{20}$$

Chambolle (2004) and Bellettini and Coscia (1994) have proven this for continuous and discretised media, respectively. For a discrete medium, i.e. when the solid is discretised into linear finite elements, Bourdin et al. (2008) have argued that a correction factor must be applied that is approximately equal to $1 + \frac{h}{4\ell}$, so that the fracture energy density in Equation (12) is replaced by the expression:

$$\mathcal{G}_c \to \left(1 + \frac{h}{4\ell}\right) \mathcal{G}_c \ . \tag{21}$$

This correction has been applied in the numerical studies of Borden et al. (2014) and May et al. (2015).

3. Numerical assessment of crack nucleation for a one-dimensional bar with a reduced cross section under tension

3.1. Previous findings

In Miehe et al. (2010b) a study has been carried out regarding the required fineness of the discretisation which is needed to properly capture a phase-field representation. It is noted that, while the study was carried out in the context of brittle crack propagation, the parametric study did not involve a coupling to the mechanical field, and purely indicates the maximum element size permitted to accurately resolve the phase field. For a two-dimensional square plate and using quadrilateral, four-noded elements it was found that a reasonable approximation of Γ by Γ_ℓ is obtained for:

$$\frac{h}{\ell} < \frac{1}{2} \ . \tag{22}$$

While this value is indicative, the limitations of the study are recalled: (i) a two-dimensional boundary value problem, (ii) simple, four-noded quadrilateral elements, and most importantly, (iii) only the phase-field was considered, not coupled to the mechanical problem of crack propagation. Likely, the criterion of Equation (22) is an upper bound, and in analyses in which the phase-field is coupled to the mechanical field, smaller values for h can be expected to be necessary.

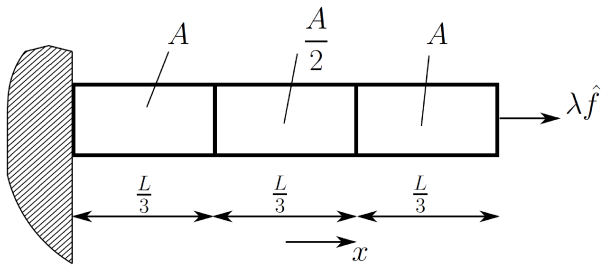

Figure 2: Bar of length L with a reduced cross section of length $L_r = L/3$ in the centre subject to a tensile load $\lambda \hat{f}$.

A study in which a coupling with the mechanical field was maintained, can be found in May et al. (2015), and Equation (22) was respected as a minimum requirement. The simple, one-dimensional boundary value problem of Figure 2 was considered. The bar under uniaxial tension is composed of a linear-elastic material, has a length $L = 1$ mm and a cross section $A = 1$ mm^2. Over L_r, the centre one-third of the bar, the cross section was reduced to $A/2$. The history field $\mathcal{H}$ is related to the elastic energy density according to Equation (19) and was used as the source term in Equation (14). For the error in the smeared approximation of the sharp crack, the following measure was taken:

$$\mathcal{E} = \frac{|\Gamma_\ell - \Gamma|}{\Gamma} \,, \tag{23}$$

where Γ_ℓ is evaluated numerically at $\max(d) = d_{\max}$ with $d_{\max} = 0.99$ and assuming that $\Gamma = A/2$ is the theoretical final crack surface. The bar was composed of a linear-elastic material with Young's modulus $E = 10$ MPa, and a fracture energy density $\mathcal{G}_c = 0.1$ Nmm^{-1}, and was discretised using one-dimensional elements.

Some remarkable observations were made:

- The error defined in Equation (23) exhibits a minimum, when plotted as a function of the internal length scale ℓ, see also the curve marked in Figure 3 by '+' symbols, which was obtained for 600 elements over the bar. For the smallest internal length scale, $\ell/L = 0.005$, this discretisation results in $h/\ell = 1/3$, thus respecting Equation (22).

- The problem persists upon mesh refinement, which is illustrated by the curved marked with 'x' symbols in Figure 3. In fact, the minimum, or

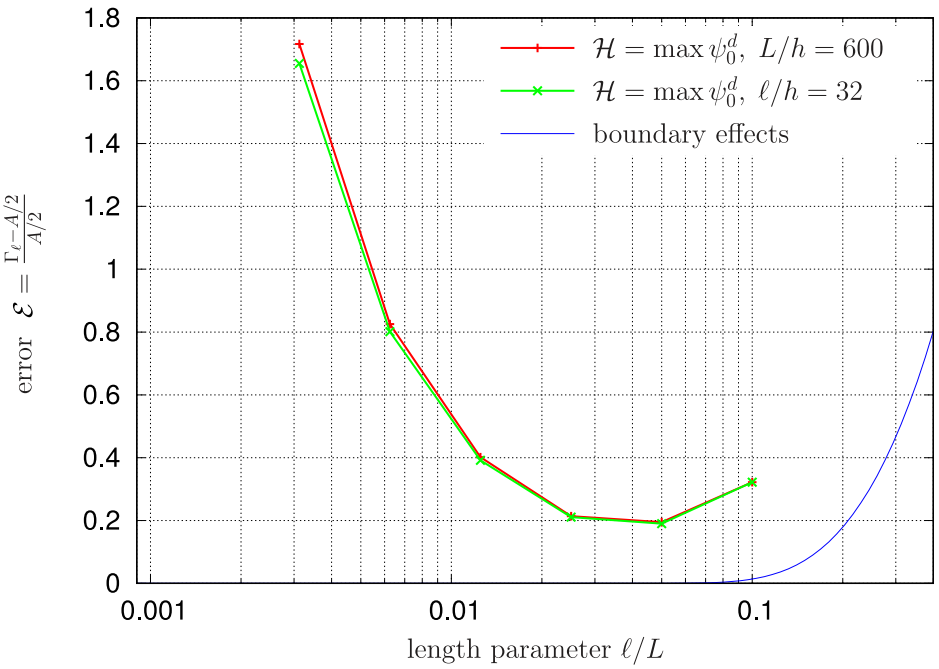

Figure 3: Convergence study for the final crack surface Γ_ℓ for a one-dimensional bar with an imperfection of length $L_r = L/3$. The calculations have been carried out for a constant element size ($L/h = 600$) and for refined meshes, with a constant ratio ($h/\ell = 1/32$) using the history field $\mathcal{H} = \max \psi^d$. In addition, the difference between the analytical solution for an infinite bar and a bar of finite length L, Equation (27), has been plotted (blue line).

smallest error that could be obtained is virtually independent of the discretisation. It is noted that the mesh size has been taken proportional to the internal length scale for this set of computations: $h/\ell = 1/32$, which leads to a mesh more than ten times as fine as the previous set of calculations for the smallest length scale $\ell/L = 0.05$.

From these computations it seems that convergence of the discretised, regularised solution is not necessarily attained, since the numerically obtained final crack surface fails to converge towards the assumed value, i.e.

$$\Gamma_\ell \Big|_{l \to 0} \neq \Gamma \ . \tag{24}$$

3.2. Boundary effects

It is noted that the theoretical results on Γ-convergence have been obtained under the assumption of an infinite medium, hence no boundary effects

were considered, while the above calculations are for a (homogeneous) bar of finite length L. To investigate the possible effects thereof, we reformulate the one-dimensional boundary condition of the infinite bar, Equation (3), as

$$d(0) = 1 \quad \text{and} \quad d(\pm L/2) = 0 \ , \tag{25}$$

which holds for a finite domain $\Omega = [-L/2; +L/2]$. The analytical solution of the differential equation, Equation (2), subject to the boundary conditions of Equation (25), reads:

$$d(x) = \frac{1}{1 - \mathrm{e}^{-\frac{L}{2\ell}}} \left(\mathrm{e}^{-\frac{|x|}{2\ell}} - \mathrm{e}^{-\frac{L}{2\ell}} \mathrm{e}^{\frac{|x|}{2\ell}} \right) \ , \tag{26}$$

and the functional for the distributed crack becomes:

$$\Gamma_\ell = \int_{-\frac{L}{2}}^{+\frac{L}{2}} \frac{1}{4\ell} \left(d^2 + 4\ell^2 {d_{,x}}^2 \right) A \mathrm{dx} = A \frac{1 - \mathrm{e}^{-\frac{L}{\ell}}}{\left(1 - \mathrm{e}^{-\frac{L}{2\ell}} \right)^2} \tag{27}$$

instead of Equation (5). Hence, the approximated crack surface depends on the length of the bar L. Accordingly, for smaller values of L, or equivalently, for larger values of ℓ/L, the *increase* in the error $\mathcal{E}$ is just a boundary effect. Indeed, when plotting the solution of Equation (26) in Figure 3, it is observed that the error does *not* increase, since the distance between this curve and the numerical solutions marked with '+' and 'x' symbols remains approximately constant.

However, Γ_ℓ as given by Equation (27) should converge to $A/2$ for $\ell/L \to 0$, which is clearly contradicted by the curves denoted by the '+' and 'x' symbols in Figure 3.

3.3. Numerical setting

In the following we use the one-dimensional problem with a reduced cross section over the centre of the bar, see Figure 2. The weak forms of the coupled system of governing equations (13), (14) subject to the boundary conditions (15), (16) are recast in matrix-vector form:

$$\delta \mathbf{u}^{\mathrm{T}} \Bigg[\underbrace{\int_\Gamma \mathbf{N}_u^{\mathrm{T}} \bar{\mathbf{t}} dA}_{\mathbf{f}_u^{\mathrm{ext}}} - \underbrace{\int_\Omega \mathbf{B}_u^{\mathrm{T}} \mathbf{C}(d) \mathbf{B}_u \mathbf{u} dV}_{\mathbf{f}_u^{\mathrm{int}}(u,d)} \Bigg] = 0 \tag{28}$$

and

$$\delta \mathbf{d}^{\mathrm{T}} \underbrace{\left[\int_{\Omega} \frac{\mathcal{G}_c}{2\ell} \left(\mathbf{N}_d^{\mathrm{T}} \mathbf{N}_d + 4\ell^2 \mathbf{B}_d^{\mathrm{T}} \mathbf{B}_d \right) \mathbf{d} + \mathbf{N}_d^{\mathrm{T}} \frac{\partial g}{\partial d} \mathcal{H} dV \right]}_{\mathbf{f}_d^{\mathrm{int}}(d,u)} = 0 \tag{29}$$

where $\mathbf{N}_u$ and $\mathbf{N}_d$ contain quadratic Lagrangian shape functions interpolating the displacement field u and the phase field d, $\mathbf{B}_u$ and $\mathbf{B}_d$ contain the derivatives of the shape functions and $\mathbf{C}(d)$ is the material stiffness matrix. The integrals are calculated numerically using a standard Gauss method with five integration points. The bar of length L is discretised such that regions of large gradients of d and u are meshed using the smallest element size h while the mesh is coarsened towards both ends of the bar.

To prevent bifurcations[1] that can occur for small internal length scales, the loading of the bar is realised by setting $u(x = -L/2) = 0$ and $\mathbf{f}_u^{\mathrm{ext}} = \lambda \hat{f}$ and introducing an arc-length method that controls the load parameter λ such that the phase-field variable at the centre of the bar $d(x = 0)$ monotonically increases at each load step[2]. Consequently, the following nonlinear system of equations

$$\begin{bmatrix} \mathbf{f}_u^{\mathrm{int}}(u,d) - \lambda \hat{f} \\ \mathbf{f}_d^{\mathrm{int}}(d,u) \\ f_{\mathrm{arc}}(d,\lambda) \end{bmatrix} = \mathbf{0}, \tag{30}$$

where $f_{\mathrm{arc}}(d,\lambda)$ denotes the arc-length function, is solved in a monolithic scheme.

3.4. Irreversibility

We recall that, following concepts borrowed from damage mechanics, Miehe et al. (2010b,a) have interpreted the phase-field variable in the variational theory of brittle fracture as a damage-like parameter, d, and have used a history field

$$\mathcal{H} = \max_{s \in [0;t]} \psi^d(\boldsymbol{\epsilon}, s) \ ,$$

[1]For a fully broken state ($d(x) = 1$) of a *homogeneous* bar of length L and a cross section A the functional (5) results in $\Gamma_\ell = \frac{AL}{4\ell}$, which can be understood as a smeared approximation of $\frac{L}{4\ell}$ *cracks*. For a discussion of the uniqueness and the stability of the homogeneous response see also (Pham et al., 2011; Pham and Marigo, 2013).

[2]For a sufficient large bar, this results in the localization of damage *in one single zone* which corresponds to the lowest energy and is associated to a snap-back as shown by (Pham and Marigo, 2013), which the authors interpret as the nucleation of a single crack.

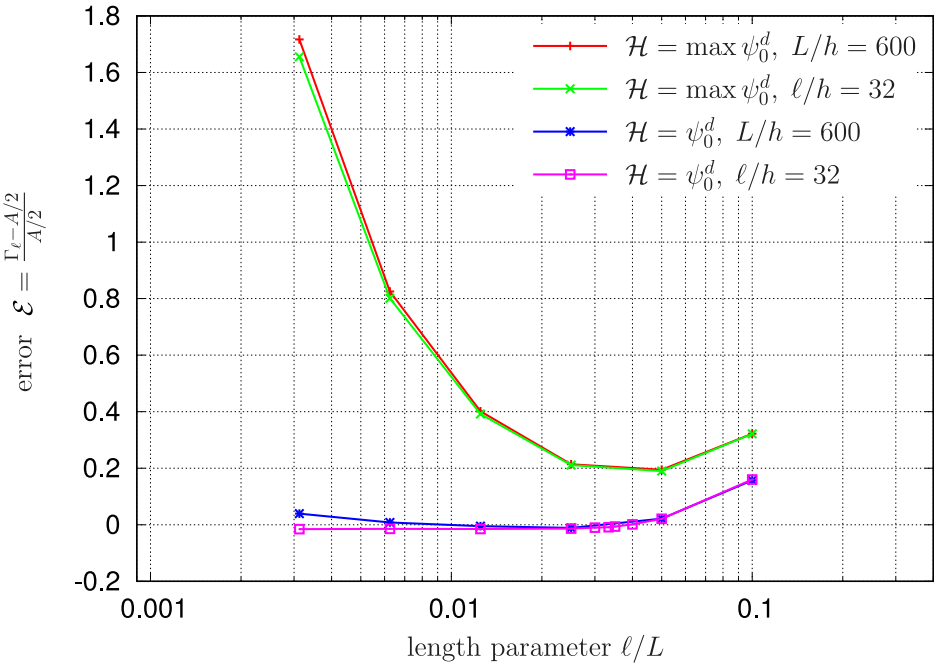

Figure 4: Convergence study for the final crack surface Γ_ℓ for a one-dimensional bar with an imperfection of length $L_r = L/3$. Two cases have been considered: (i) $\mathcal{H} = \max \psi^d$ and (ii) $\mathcal{H} = \psi^d$. The calculations have been carried out for a constant element size ($L/h = 600$) and for refined meshes, with a constant ratio ($h/\ell = 1/32$).

cf. Equation (19), to enforce irreversibility of damage:

$$\dot{d} \geq 0 \ . \tag{31}$$

Now, we investigate numerically the consequences of the constraint of Equation (19), and do so by dropping the requirement of irreversibility, and just assign the *current* value of $\psi^d(\boldsymbol{\epsilon})$ to the history field:

$$\mathcal{H} = \psi^d(\boldsymbol{\epsilon}) \ . \tag{32}$$

The results denoted by the curve with the stars in Figure 4 show that the errors then virtually disappear. Evidently, the errors due to the boundary effect for small values of L are still present, and on the other side, i.e. for small ℓ/L, discretisation errors emerge when the heuristic limit for the element size of Equation (22) is approached. In line with earlier comments, this indicates that the condition of Equation (22) is to be conceived as an upper bound

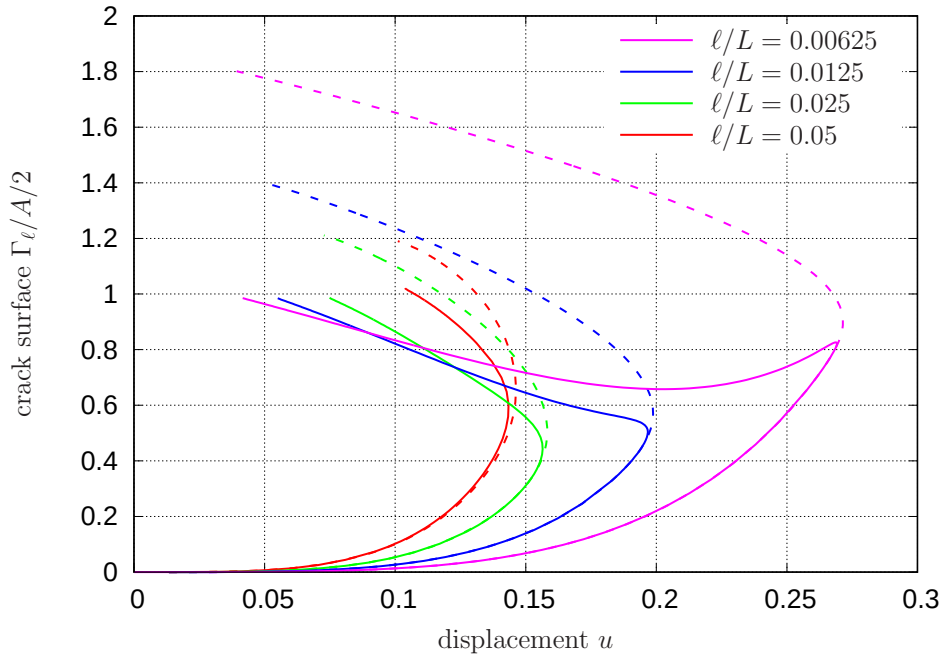

Figure 5: Crack surface Γ_ℓ - displacement curves ($d_{\max} = 0.99$, element size $\ell/h = 32$, length of imperfection $L_r = L/3$; dashed: $\mathcal{H} = \max \psi^d$, solid lines: $\mathcal{H} = \psi^d$).

to the element size, and that in practice smaller values should be adopted. When using a much finer mesh ($h/\ell = 1/32$), the curve marked with squares is obtained, which does not exhibit an increase in the error $\mathcal{E}$ for small values of the internal length scale ℓ, and levels off, albeit at a very small non-zero value.

In order to understand these differences, it is instructive to compare the evolution of the numerically calculated crack surface Γ_ℓ, Figure 5. Little difference is observed until peak load, but thereafter a markedly different behaviour is found. This is most pronounced for smaller values for the internal length scale, which yield narrow crack zones and very brittle behaviour. For instance, for the smallest considered value of the dimensionless internal length scale – $\ell/L = 0.00625$ – the numerically evaluated crack surface Γ_ℓ exceeds the assumed value $A/2$ at peak load by approximately 50 % for both expressions of the history field. But the evolution of the crack surface Γ_ℓ differs significantly after peak load. For $\mathcal{H} = \max \psi^d$, Γ_ℓ cannot decrease. On the contrary, it exhibits a further, monotonic increase even though at peak load the assumed value had already been exceeded, yielding highly er-

roneous results. On the other hand, not enforcing a non-decreasing value of d, allows Γ_ℓ to decrease. This indeed happens, and Γ_ℓ ultimately converges to approximately $A/2$:

$$\Gamma_\ell\Big|_{l\to 0} = A/2. \tag{33}$$

Note that the although condition (31) is not enforced for $\mathcal{H} = \psi^d$ (solid lines in Figure 5), there are some settings where (33) holds and the numerically calculated crack surface Γ_ℓ monotonically increases, i.e.

$$\dot{\Gamma}_\ell \geq 0 \tag{34}$$

for the whole loading process. Further note that (34) is an integral-type condition for crack *growth* (Bourdin et al., 2000), while (31) locally ensures the irreversibility of d as a damage-like parameter and thus enforces (34) (Miehe et al., 2010a). However there is no apparent reason that either (31) or (34) apply for the studied case of the *nucleation of a single crack*, while (33) needs to be fulfilled.

The error in the approximated crack surface is directly related to the distribution of the phase-field variable along the bar. At peak load the distribution is almost equal for both expressions of the history field, Figure 6. As expected, the phase-field variable d is smeared over the imperfection for larger values of ℓ/L, whereas smaller values of ℓ/L result in a markedly sharper profile. It is emphasised that Figure 6 clearly shows that a fully broken state, i.e. $d = 1$, is *not* obtained at peak load. Also, $d \neq 0$ for $x = \pm L/2$, even for large values of L, although d then becomes smaller at the ends of the bar.

At continued loading, the distribution of the phase-field variable starts to differ, depending on the expression for the history field. For $\mathcal{H} = \max \psi^d$ the phase-field variable cannot decrease which results in a profile that is significantly broader than the profile which is obtained when $\mathcal{H} = \psi^d$ is utilised, see Figure 7. Again, preventing d to decrease seems to prohibit the formation of a sharp single crack in the sense of Equation (1) with $d = 0$ for $x = \pm L/2$ and $d(0) = d_{\max}$.

These observations also hold for different imperfection lengths as long as $L_r/\ell > 8$ (approximately), see Figure 8. This corresponds to the discussion of boundary effects, as the error for smaller values $L_r/L < 8$ is related to Equation (27) for a finite domain $\Omega = [-L_r/2; +L_r/2]$.

The influence of the discretisation is shown in Figure 9, where the error $\mathcal{E}$ is plotted as a function of the dimensionless size h/ℓ. For the ratio $h/\ell = 0.05$

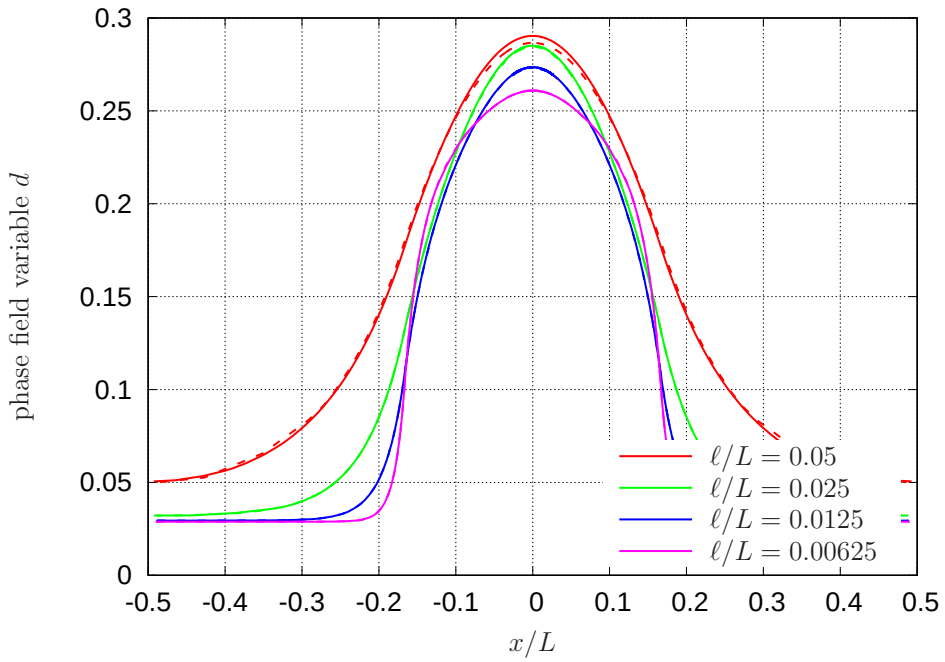

Figure 6: Distribution of the phase-field parameter d along the bar at peak load (element size $h/\ell = 32$). The dashed lines are for $\mathcal{H} = \max \psi^d$, and the solid lines represent the cases for which $\mathcal{H} = \psi^d$.

the error converges to a small positive value, since the crack is smeared into the region with the full cross section of A. On the contrary, a sharp profile located almost completely *inside* the region with a reduced cross section of $A/2$ evolves for small values of l/L (see Figure 7) and thus the error converges to a very small negative value. Figure 10 shows that it is, in fact, the value of $d_{\max}$ where Γ_ℓ is evaluated, determines the exact value to which $\mathcal{E}$ converges.

Figure 11 shows that the load-displacement curves do not differ markedly when either requiring $\mathcal{H} = \max \psi^d$, or using $\mathcal{H} = \psi^d$ until the peak load has been reached. However, a much more brittle failure behaviour, with a concomitant pronounced snap-back behaviour is observed for $\mathcal{H} = \psi^d$, i.e. when the largest attained value of ψ^d is not treated as a history variable.

4. Concluding remarks

Phase-field approaches for brittle fracture can be very powerful when it comes to capturing complex two and three-dimensional crack patterns,

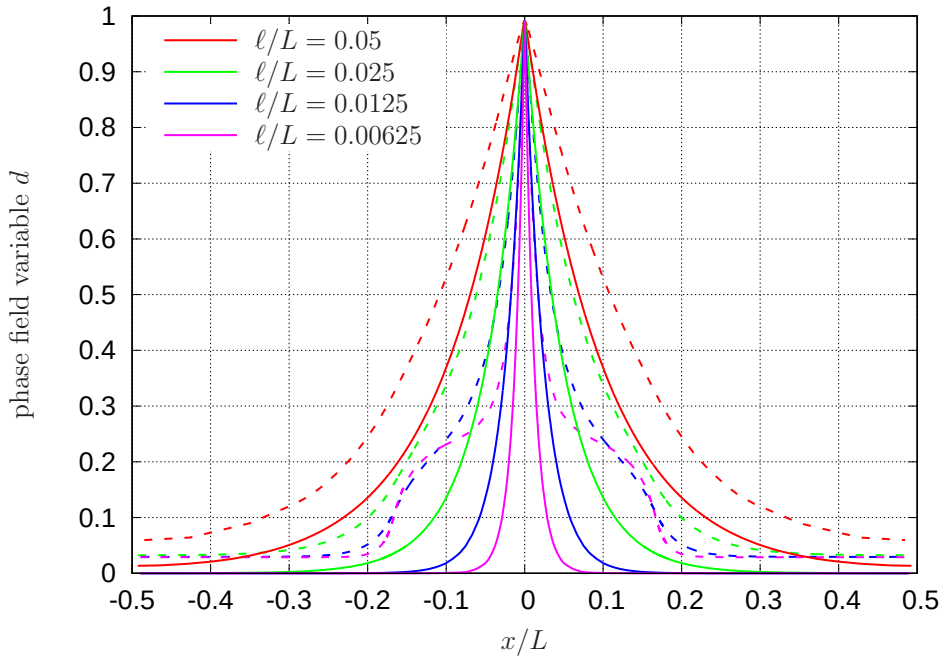

Figure 7: Distribution of the phase-field parameter d along the bar at $d_{\max} = 0.99$ (element size $h/\ell = 32$). The dashed lines are for $\mathcal{H} = \max \psi^d$, and the solid lines represent the cases for which $\mathcal{H} = \psi^d$.

including phenomena like crack branching and kinking.

A natural requirement is that the functional that describes the smeared crack surface, converges to the original functional that describes the discrete crack surface. While proofs for this so-called Γ-convergence have been given (Bellettini and Coscia, 1994; Chambolle, 2004), doubt has arisen whether Γ-convergence can actually be achieved in numerical computations where both the internal length scale and the spacing of the discretisation are small, but finite (Vignollet et al., 2014; May et al., 2015).

By taking the example of a simple, one-dimensional bar with an imperfection in the centre, we have shown that the discrepancies between the theoretical proofs and actual computations stem from two different causes, both leading to a distortion of the original exponential regularisation profile.

First, there is the effect of a finite specimen length in numerical computations. When a correction is made for the fact that specimens have a finite length, and the appropriate boundary conditions are imposed, the numerical solutions tend to replicate the analytical solution for specimens which are

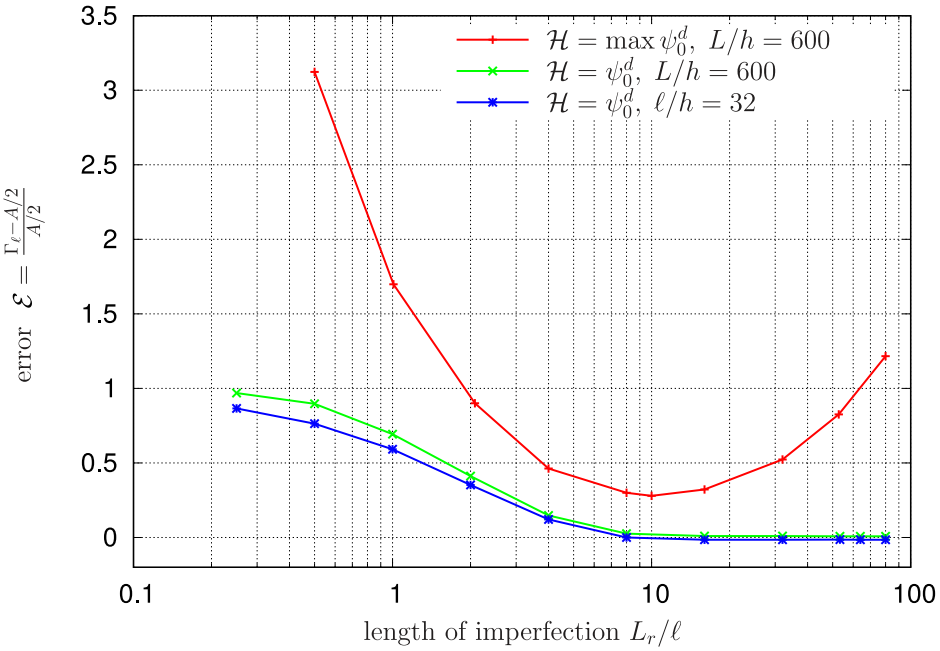

Figure 8: Error $\mathcal{E}$ for different imperfection lengths ($d_{\max} = 0.99$, $\ell/L = 0.00625$)

short relative to the value of the internal length scale.

A more fundamental problem resides in the damage-like formulation of the variational theory of brittle fracture, which recently has become en vogue (Miehe et al., 2010b,a). This damage-like format heuristically introduces a degradation function, which it identifies with the phase-field parameter. Moreover, to enforce irreversibility of this damage parameter, a history field $\mathcal{H}$ is normally introduced, which equivalences the locally attained maximum value of the damage parameter to the history parameter, thus preventing the phase-field parameter from reducing. A monotonically increasing order parameter seems to prevent the construction of a proper functional, and would therefore invalidate a basic assumption of the theory on which the convergence proofs are based.

The numerical studies presented herein corroborate this reasoning. After reaching the peak load the functional of the smeared crack decreases to asymptotically reach the discrete value without the introduction of a constraint that prevents the phase-field variable from decreasing locally. On the other hand, it cannot decrease, and actually continues to grow, when such a constraint is introduced in the form of a history variable, leading to errors

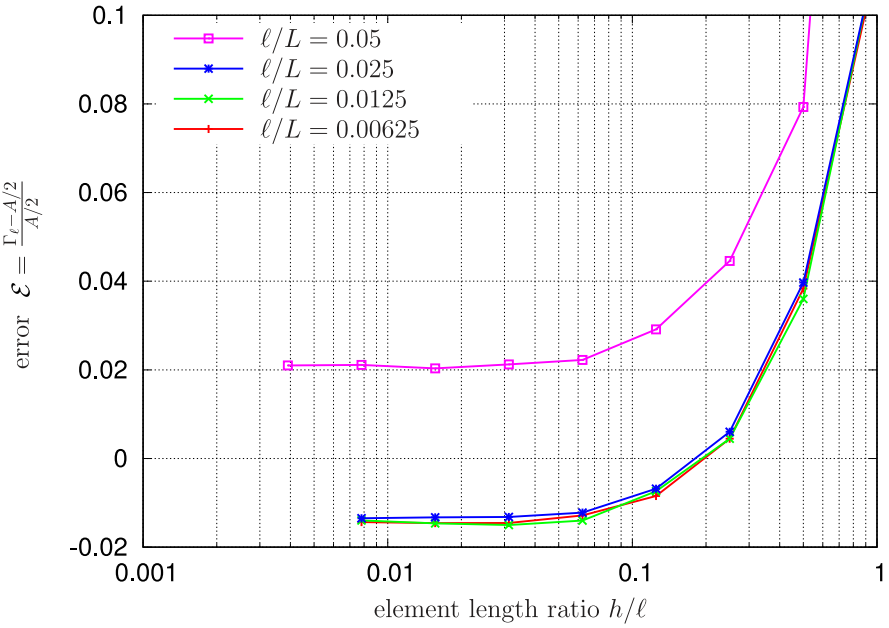

Figure 9: Influence of the mesh size on the error $\mathcal{E}$ for $\mathcal{H} = \psi^d$.

that may amount up to 100 %, depending on the parameters chosen.

The question is whether phase-field approaches for brittle fracture should be augmented such that irreversibility is ensured in some way. If so, then an approach that pins the phase-field variable to a fixed value close to one when a certain threshold value has been exceeded (Bourdin et al., 2000; Kuhn and Müller, 2010) is to be preferred to a damage-like constraint in the sense of Miehe et al. (2010b,a).

Acknowledgement

The first three authors gratefully acknowledge support by the Deutsche Forschungsgemeinschaft in the Priority Program 1748 "Reliable simulation techniques in solid mechanics. Development of non-standard discretisation methods, mechanical and mathematical analysis" under the project KA3309/3-1. The last author was supported by the European Research Council (ERC Advanced Grant 664734 "PoroFrac").

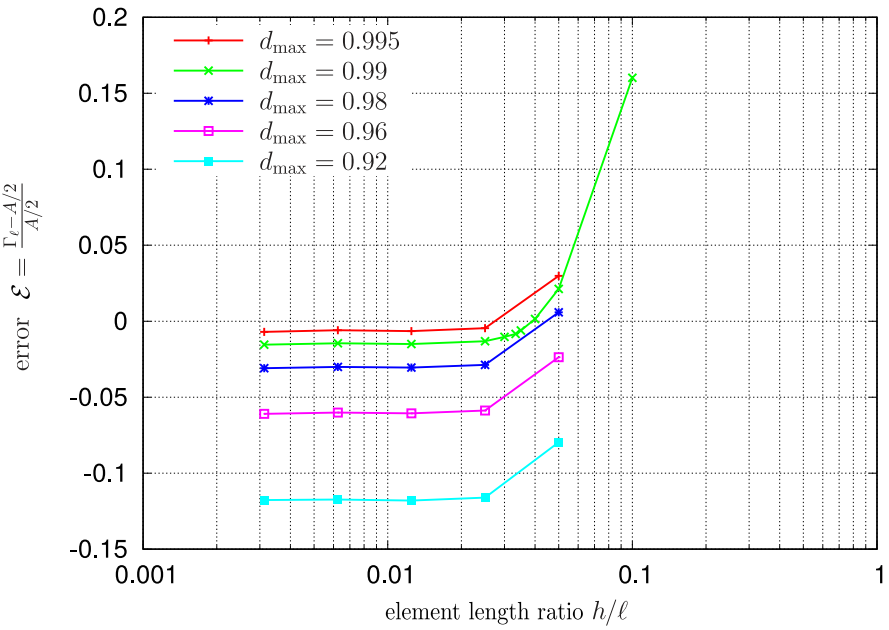

Figure 10: Influence of $d_{\max}$ and the element length ratio h/ℓ on the error $\mathcal{E}$ for $\mathcal{H} = \psi^d$.

References

Amor, H., Marigo, J.J., Maurini, C., 2009. Regularized formulation of the variational brittle fracture with unilateral contact: Numerical experiments. Journal of the Mechanics and Physics of Solids 57, 1209–1229.

Bellettini, G., Coscia, A., 1994. Discrete approximation of a free discontinuity problem. Discrete Functional Analysis and Optimization 15, 201–224.

Belytschko, T., Black, T., 1999. Elastic crack growth in finite elements with minimal remeshing. International Journal for Numerical Methods in Engineering 45, 601–620.

Borden, M.J., Hughes, T.J.R., Landis, C.M., Verhoosel, C.V., 2014. A higher-order phase-field model for brittle fracture: Formulation and analysis within the isogeometric analysis framework. Computer Methods in Applied Mechanics and Engineering 273, 100–118.

Borden, M.J., Verhoosel, C.V., Scott, M.A., Hughes, T.J.R., Landis, C.M., 2012. A phase-field description of dynamic brittle fracture. Computer Methods in Applied Mechanics and Engineering 217-220, 77–95.

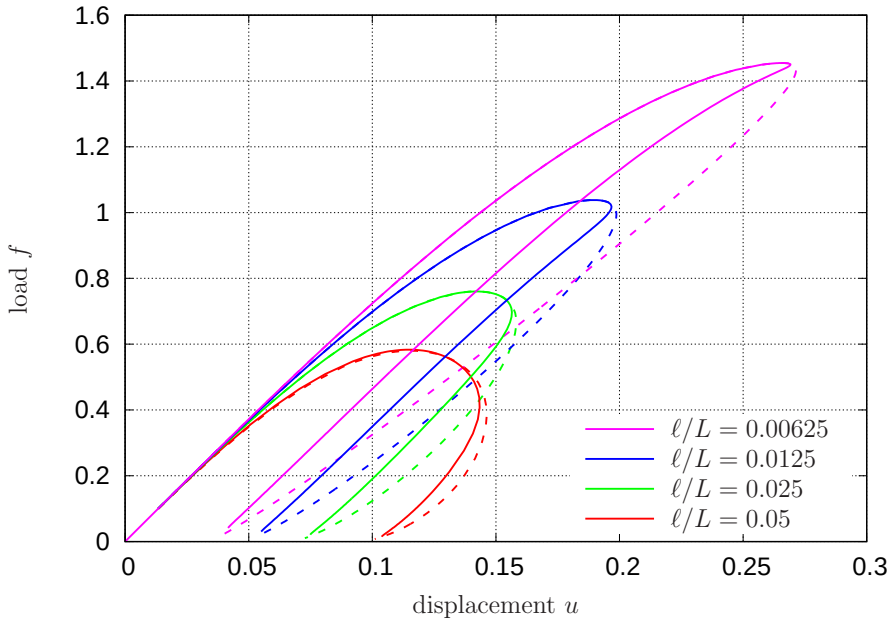

Figure 11: Load - displacement curves for $d_{\max} = 0.99$, element size $h/\ell = 1/32$. The dashed lines are for $\mathcal{H} = \max \psi^d$, while the solid lines relate to $\mathcal{H} = \psi^d$. For both formulations snap-back behaviour is observed, which is more pronounced for $\mathcal{H} = \psi^d$. For both formulations, snap-back behaviour is observed, which can be traced because of the adopted path-following method, but for $\mathcal{H} = \psi^d$ the behaviour is much more brittle. It is noted that for both cases there is continued loading in the centre of the bar.

de Borst, R., Benallal, A., Heeres, O.M., 1996. A gradient-enhanced damage approach to fracture. Journal de Physique IV C6, 491–502.

de Borst, R., Réthoré, J., Abellan, M.A., 2006. A numerical approach for arbitrary cracks in a fluid-saturated medium. Archive of Applied Mechanics 75, 595–606.

de Borst, R., Verhoosel, C.V., 2016. Gradient damage vs phase-field approaches for fracture: Similarities and differences. Computer Methods in Applied Mechanics and Engineering 312, 78–94.

Bourdin, B., 2007. Numerical implementation of the variational formulation for quasi-brittle fracture. Interfaces and Free Boundaries 9, 411–430.

Bourdin, B., Francfort, G.A., Marigo, J.J., 2000. Numerical experiments in

revisited brittle fracture. Journal of the Mechanics and Physics of Solids 48, 797–826.

Bourdin, B., Francfort, G.A., Marigo, J.J., 2008. The variational approach to fracture. Journal of Elasticity 91, 5–148.

Camacho, G.T., Ortiz, M., 1996. Computational modeling of impact damage in brittle materials. International Journal of Solids and Structures 33, 1267–1282.

Chambolle, A., 2004. An approximation result for special functions with bounded deformation. Journal de Mathématiques Pures et Appliquées 83, 929–954.

Chen, L.Q., 2002. Phase-field models for microstructure evolution. Annual Reviews of Materials Research 32, 113–140.

Emmerich, H., 2008. Advances of and by phase-field modelling in condensed matter physics. Advances in Physics 57, 1–87.

Francfort, G.A., Marigo, J.J., 1998. Revisiting brittle fracture as an energy minimization problem. Journal of the Mechanics and Physics of Solids 46, 1319–1342.

Frémond, M., Nedjar, B., 1996. Damage, gradient of damage and principle of virtual power. International Journal of Solids and Structures 33, 1083–1103.

Hesch, C., Gil, A., Ortigosa, R., Dittmann, M., Bilgen, C., Betsch, P., Franke, M., Janz, A., Weinberg, K., 2017. A framework for polyconvex large strain phase-field methods to fracture. Computer Methods in Applied Mechanics and Engineering 317, 649 – 683.

Hofacker, M., Miehe, C., 2013. A phase field model of dynamic fracture: Robust field updates for the analysis of complex crack patterns. International Journal for Numerical Methods in Engineering 93, 276–301.

Kästner, M., Metsch, P., de Borst, R., 2016. Isogeometric analysis of the Cahn-Hilliard equation – A convergence study. Journal of Computational Physics 305, 360–371.

Kuhn, C., Müller, R., 2010. A continuum phase-field model for fracture. Engineering Fracture Mechanics 77, 3625–3634.

May, S., Vignollet, J., de Borst, R., 2015. A numerical assessment of phase-field models for brittle and cohesive fracture: Γ-convergence and stress oscillations. European Journal of Mechanics - A/Solids 52, 72 – 84.

Miehe, C., Hofacker, M., Welschinger, F., 2010a. A phase field model for rate-independent crack propagation: Robust algorithmic implementation based on operator splits. Computer Methods in Applied Mechanics and Engineering 199, 2765–2778.

Miehe, C., Welschinger, F., Hofacker, M., 2010b. Thermodynamically consistent phase-field models of fracture: Variational principles and multi-field fe implementations. International Journal for Numerical Methods in Engineering 83, 1273–1311.

Moelans, N., Blanpain, B., Wollants, P., 2008. An introduction to phase-field modelling of microstructure evolution. Calphad 32, 268–294.

Moës, N., Dolbow, J., Belytschko, T., 1999. A finite element method for crack growth without remeshing. International Journal for Numerical Methods in Engineering 46, 131–150.

Mumford, D., Shah, J., 1989. Optimal approximations by piecewise smooth functions and associated variational problems. Communications on Pure and Applied Mathematics 42, 577–685.

Peerlings, R.H.J., de Borst, R., Brekelmans, W.A.M., de Vree, J.H.P., 1996. Gradient enhanced damage for quasi-brittle materials. International Journal for Numerical Methods in Engineering 39, 3391–3403.

Pham, K., Marigo, J.J., 2013. From the onset of damage to rupture: construction of responses with damage localization for a general class of gradient damage models. Continuum Mechanics and Thermodynamics 25, 147–171.

Pham, K., Marigo, J.J., Maurini, C., 2011. The issues of the uniqueness and the stability of the homogeneous response in uniaxial tests with gradient damage models. Journal of the Mechanics and Physics of Solids 59, 1163 – 1190.

Secchi, S., Simoni, L., Schrefler, B.A., 2007. Mesh adaptation and transfer schemes for discrete fracture propagation in porous materials. International Journal for Numerical and Analytical Methods in Geomechanics 31, 331–345.

Steinbach, I., 2009. Phase-field models in materials science. Modelling and Simulation in Materials Science 17, 073001.

Verhoosel, C.V., de Borst, R., 2013. A phase-field model for cohesive fracture. International Journal for Numerical Methods in Engineering 96, 43–62.

Vignollet, J., May, S., de Borst, R., Verhoosel, C.V., 2014. Phase-field models for brittle and cohesive fracture. Meccanica 49, 2587–2601.

Wawrzynek, P.A., Ingraffea, A.R., 1987. Interactive finite element analysis of fracture processes: an integrated approach. Theoretical and Applied Fracture Mechanics 8, 137–150.

Wells, G.N., de Borst, R., Sluys, L.J., 2002. A consistent geometrically non-linear approach for delamination. International Journal for Numerical Methods in Engineering 54, 1333–1355.